DOI: 10.3901/CJME.2011.**.***, available online at www.cjmenet.com; www.cjmenet.com.cn

Flow Field Characteristics for Parachute-projectile System

ZHU Yong*, LIU Li, and WANG Zhengping

School of Aerospace Engineering, Beijing Institute of Technology, Beijing 100081, China

Received January 26, 2010; revised December 6, 2010; accepted February, 2011; published electronically February, 2011

Abstract: In the current research for parachute flow field nowadays, the size of parachutes in previous research are so large compared with their carriers that the effects of the carriers wake flow to parachute are always neglected. Different from such large parachutes, the parachute size in this paper is on the same magnitude with the carrier, thus, the carrier can obviously affect the parachute flow field. In this paper, flow field characteristics of small parachute for projectile decelerating are researched through two approaches, namely, computational fluid dynamics (CFD) simulation and wind tunnel tests. Three parachutes with various sizes are chosen for study. Firstly, the CFD simulation of flow field around these parachutes is carried out, and then the CFD simulation of parachute-projectile systems is executed. According to the simulation results, the phenomenon is observed that in the simulations of parachutes there are two vortex-rings at the wind shadow of parachutes, however, in the second simulations of parachute-projectile systems, two additional vortex-rings emerge inside the parachutes. Due to these two inner vortex-rings, the pressure inside parachutes decreases. As a result, the drag of parachute in simulation of parachute-projectile systems is about 20% smaller compared with the prior one. In order to verify the numerical results of CFD simulations, wind tunnel tests are employed. In terms of the data of the wind tunnel tests, the CFD simulation for flow field characteristics is reasonable and feasible. The results of both CFD simulation and wind tunnel tests demonstrated the influence of projectile wake flow to parachute drag can not be neglected if the parachute size is on the same magnitude with projectile. The influence to parachute drag from the ratio of projectile diameter to parachute diameter is also analyzed both in CFD simulations and wind tunnel tests. The approach combined CFD simulation and wind tunnel tests proposed can be used to guide the design of such parachute whose size is on the same magnitude with carrier.

Key words: parachute, projectile, flow field, computational fluid dynamics (CFD), wind tunnel test

1 Introduction

Parachute is one of the most important tools for deceleration due to its large drag for decelerating, research on flow field characteristics is one of the key points in such domain. Because of the flexibility and permeability of parachute, accurate description of parachute mechanical properties is quite difficult, which is also an interesting issue on flow field characteristics research for parachute. Nowadays, the methods based on semi-theory and semi-experiment have been widely used in parachute design, whereas, many problems have been found in such approaches[1–4]. Along with the development of computational fluid dynamics(CFD) and computer technology, more and more researchers concentrated on using CFD simulation to describe flow field characteristics for parachute. Based on the results of CFD simulation, on one side, fluid-structure interaction simulation can be used to solve many complex problems such as inflation, wake re-contact[5–7]. On the other side, it can be combined with the parachute dynamic models to analyze the dynamics questions more accurately[8–9].

So far, many achievements have been obtained in the researches for parachute flow field. KEITH, et al[10], presented a parallel computational technique to carry out three-dimensional simulations of parachute fluid-structure interactions in 2001. TAYLOR[11] studied the fluid-structure interaction simulation to investigate the apparent mass dynamic loading of parachute in 2003. JOHARI, et al[12], gave one coupled fluid-structure parachute inflation model to discover flow physics about inflating model parachute canopies in 2003, and used this model to obtain the opening force of parachute in 2007[13]. CAO, et al[14], proposed a numerical simulation method of parachute fluid-structure interaction problem using semi-implicit method for pressure-linked equations algorithm to compute parachute fluid-structure interaction and did parachute flow field analysis in 2007. JIANG[15], et al, established a fluid dynamics computational model and solved RNG k-ε turbulence N-S equation to find the wake topological structure of an axisymmetrical parachute in 2005, and used this fluid dynamics computational model to research the influence of circular angle in symmetric plane to flow field characteristics of an axisymmetrical parachute in 2006[16]. WANG[17], et al, did a numerical simulation of parachute fluid-solid coupling problem using semi-implicit method

* Corresponding author. E-mail: zhuyong@bit.edu.cn

for pressure-linked equations algorithm in 2007. SONG, et al[18], established a fluid-structure interaction simulation method to simulate the stage of hemispherical parachute stable descent in 2009. VLADIMYR, et al[19], did a simulation of fluid-structure interaction and compared it with wind tunnel tests in 2009.

Compared with their carriers, the sizes of such parachutes in papers above are usually so large that the effects of the carriers wake flow to parachute are neglected. For this reason, researchers only calculated flow field around parachute alone. However, the parachute in this paper is used for projectile deceleration. Different from the large parachute in previous papers, it is much smaller and always works in subsonic. The problems of inflation and wake re-contact are not very obvious and can be neglected, but the wake flow of projectile will affect the parachute flow field obviously, as the parachute size is on the same magnitude with projectile. It is necessary to research flow field around both parachute and projectile. In this paper, in order to reveal the influence of projectile to parachute, the CFD simulation of flow field around parachute is carried out and the CFD simulation of flow field around parachute-projectile system is implemented, respectively. The wind tunnel tests for these two situations are also adopted to verify the results of CFD simulation.

2 Computation Scheme

2.1 Geometry model

Three "six sections" hemispherical parachutes models are built in this paper. They are shown in Fig. 1 and their parameters are shown in Table 1.

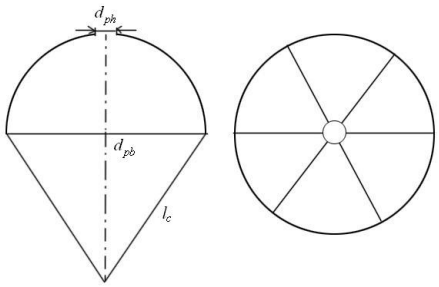

Fig. 1. Sketches of hemispherical parachute

Table 1. Parameters of hemispherical parachute

Parameter	Parachute A	Parachute B	Parachute C
Parachute bottom diameter d_{pb}/m	1.06	0.96	0.85
Parachute top hole diameter d_{ph}/m	0.085	0.077	0.068
Parachute area A_p/m^2	0.882	0.724	0.567
Cord lenth l_c/m	0.84	0.81	0.78

The ratio of top holes diameter to parachute bottom diameter is constant, that is

$$\frac{d_{phA}}{d_{pbA}}=\frac{d_{phB}}{d_{pbB}}=\frac{d_{phC}}{d_{pbC}}. \tag{1}$$

The cord length l_c can be calculated from Eq. (2), so that the distance between three parachutes and projectile is constant.

$$l_{cA}^2-\left(\frac{d_{pbA}}{2}\right)^2=l_{cA}^2-\left(\frac{d_{pbA}}{2}\right)^2=l_{cA}^2-\left(\frac{d_{pbA}}{2}\right)^2. \tag{2}$$

The projectile is shown in Fig. 2 and its parameters are shown in Table 2.

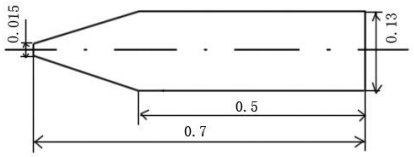

Fig. 2. Sketches of projectile

Table 2. Parameters of projectile

Projectile body diameter d_{sb}/m	Projectile head diameter d_{sh}/m	Projectile body length l_{sb}/m	Projectile head length l_{sh}/m
0.13	0.015	0.7	0.2

2.2 Hypothesis

In order to build the parachute model, some hypothesizes are given.

(1) Thin films canopy hypothesis: Since the thickness of canopy does not influence flow field calculation, it is hypothesized as zero.

(2) Non-permeable canopy hypothesis: The canopy is weaved closely and the permeability of canopy is hypothesized as zero.

(3) Steady flow field hypothesis: As the role of parachute top hole, the unstable periodical and non-periodical vortex-rings are avoided, stability of parachute is increased, and the unsteady effect of flow field is weakened obviously. The flow field is hypothesized as steady.

(4) Incompressible flow field hypothesis: Because the steady velocity of parachute is lower than 15 m/s, the flow field is typical incompressible type.

(5) Other hypothesis: The attack angle of parachute is hypothesized as zero and the shape of parachute is axisymmetrical.

2.3 Incompressible Navier-Stokes equations

The steady velocity of parachute is lower than 15 m/s, so that flow field is typical incompressible type. Flow field around the parachute and projectile is simulated through the incompressible Navier-Stokes equations solution.

Let $\Omega_t \subset \mathbf{R}^{n_{sd}}$ and (0, T) be the spatial and temporal domains, respectively, where n_{sd} is the number of space dimensions, and let Γ_t denote the boundary of Ω_t. The spatial and temporal coordinates are denoted by $x=(x, y, z)$

and $t \in (0, T)$. The Navier-Stokes equations of incompressible flows are

$$\rho\left(\frac{\partial \boldsymbol{u}}{\partial t} + \boldsymbol{u} \cdot \nabla \boldsymbol{u} + \boldsymbol{F}\right) - \nabla \cdot \boldsymbol{\sigma} = 0, \text{ on } \Omega_t, \forall t \in (0, T), \quad (3)$$

$$\nabla \cdot \boldsymbol{u} = 0, \text{ on } \Omega_t, \forall t \in (0, T), \quad (4)$$

where ρ, $\boldsymbol{u}$, $\boldsymbol{F}$ and $\boldsymbol{\sigma}$ are the density, velocity, external body force, and stress tensor, respectively[10], and

$$\boldsymbol{\sigma}(p, \boldsymbol{u}) = pI + 2(\mu + \mu_t)\varepsilon(\boldsymbol{u}), \quad (5)$$

$$\varepsilon(\boldsymbol{u}) = \frac{1}{2}[(\nabla \boldsymbol{u}) + (\nabla \boldsymbol{u})^{\mathrm{T}}], \quad (6)$$

where p, I and μ are pressure, characteristic tensor, molecular viscosity coefficient, respectively, $\varepsilon(\boldsymbol{u})$ is strain-rate tensor. μ_t is turbulent viscosity coefficient, which can be solved from turbulence model.

2.4 Turbulence model

In this paper, the Reynolds number $Re > 10^6$, (characteristic length is equivalent bottom diameter of hemispherical parachute), so that the whole flow field of parachute is fully turbulence. Spalart-Allmaras model is used as turbulence model.

The Spalart-Allmaras turbulence model is one relatively simple one-equation model that solves a modeled transport equation for the kinematical eddy (turbulent) viscosity. This embodies a relatively new class of one-equation models in which it is not necessary to calculate a length scale related to the local shear layer thickness. The Spalart-Allmaras model was designed specifically for aerospace applications involving wall-bounded flows and has been shown to give good results for boundary layers subjected to adverse pressure gradients. It is a good choice for relatively crude simulations on coarse meshes where accurate turbulent flow computations are not critical.

$$\frac{\partial}{\partial t}(\rho\tilde{\nu}) + \frac{\partial}{\partial x_i}(\rho\tilde{\nu}u_i) = G_\nu + \frac{1}{\sigma_{\tilde{\nu}}}\left\{\frac{\partial}{\partial x_i}\left[(\mu + \rho\tilde{\nu})\frac{\partial \tilde{\nu}}{\partial x_j}\right] + C_{b2}\rho\left(\frac{\partial \tilde{\nu}}{\partial x_j}\right)^2\right\} - Y_\nu + S_{\tilde{\nu}}, \quad (7)$$

where G_ν is the production of turbulent viscosity, and Y_ν is the destruction of turbulent viscosity that occurs in the near-wall region due to wall blocking and viscous damping. $\sigma_{\tilde{\nu}}$ and C_{b2} are constants and ν is the molecular kinematical viscosity. $S_{\tilde{\nu}}$ is a user-defined source term.

The turbulent viscosity μ_t, is computed from

$$\mu_t = \rho\tilde{\nu}f_{\nu 1}, \quad (8)$$

where $f_{\nu 1}$ is the viscous damping function, and can be given by

$$f_{\nu 1} = \frac{X^3}{\chi^3 + C_{\nu 1}^3}, \quad (9)$$

$$\chi \equiv \frac{\tilde{\nu}}{\nu}. \quad (10)$$

The production term G_ν is modeled as

$$G_\nu = C_{b1}\rho\tilde{S}\tilde{\nu}, \quad (11)$$

where

$$\tilde{S} = S + \frac{\nu}{\kappa^2 d^2}f_{\nu 2}, \quad (12)$$

$$f_{\nu 2} = 1 - \frac{X}{1 + \chi f_{\nu 1}}. \quad (13)$$

C_{b1} and κ are constants, d is the distance from the wall, S is a scalar measure of the deformation tensor, and

$$S \equiv \sqrt{2\Omega_{ij}\Omega_{ij}}, \quad (14)$$

where Ω_{ij} is the mean rate-of-rotation tensor and is defined by

$$\Omega_{ij} = \frac{1}{2}\left(\frac{\partial u_i}{\partial x_j} - \frac{\partial u_j}{\partial x_i}\right). \quad (15)$$

If the effect of mean strain on the turbulence production has been taken into account,

$$S \equiv |\Omega_{ij}| + C_{\text{prod}} \min(0, |S_{ij}| - |\Omega_{ij}|), \quad (16)$$

where

$$C_{\text{prod}} = 2.0, |\Omega_{ij}| = \sqrt{2\Omega_{ij}\Omega_{ij}}, |S_{ij}| = \sqrt{2S_{ij}S_{ij}},$$

with the mean strain rate S_{ij}, defined as

$$\Omega_{ij} = \frac{1}{2}\left(\frac{\partial u_i}{\partial x_j} - \frac{\partial u_j}{\partial x_i}\right). \quad (17)$$

2.5 Computational mesh

Computational mesh can be divided into structured mesh, non-structured mesh and self-adaptive Cartesian mesh, etc. Structured mesh is employed in this paper, which is one mature technology and can be generated by many grid generation tools. The spacing rate of meshes is set up reasonably according to curvature of the surface and flow

field variation. Properties of flow field variation will be reflected through the structured mesh sufficiently and exactly.

Since both the parachute and projectile are axisymmetrical, only one quarter of them are modeled during the mesh generation. The surface meshes of parachute are shown in Fig. 3 and the surface meshes of projectile are shown in Fig. 4.

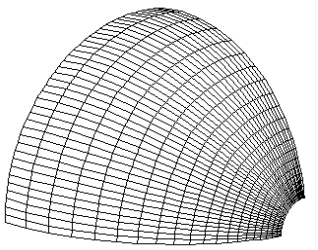

Fig. 3.　Surface meshes of parachute

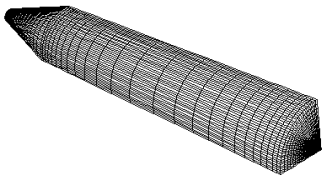

Fig. 4.　Surface meshes of projectile

2.6　Boundary conditions

The models of parachute and projectile are calculated in Fluent 6.3 environment. Boundary conditions are set up as

(1) Ideal gas model is chosen, and gas parameters keep consistent with the data from gas manual.

(2) The surface of parachute and projectile is set up as wall condition without sliding; the far field is set up as pressure far field condition; and the symmetry plane is set up as symmetry condition.

3　Numerical Result and Flow Field Characteristics Analysis

The following two numerical examples are calculated in this paper.

(1) Flow field around parachute alone is calculated, and the computational meshes are shown in Fig. 5. The number of computational meshes is 324 000.

(2) Flow field around parachute-projectile system is calculated, and the computational meshes are shown in Fig. 6. The number of computational meshes is 540 000.

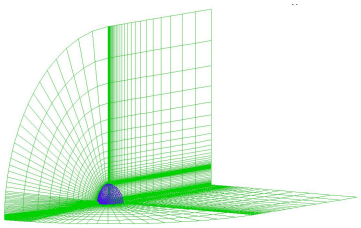

Fig. 5.　Computational meshes of parachute

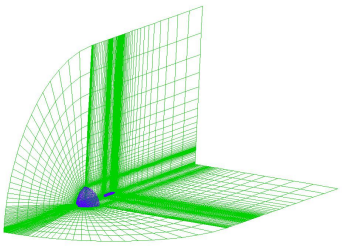

Fig. 6.　Computational meshes of parachute-projectile

The flow lines on symmetry plane of the first example are shown in Fig. 7. There are two vortex-rings in the wind shadow of parachute. Airflow breaks up into two on the inner surface of parachute. One flows through the top hole of parachute and separates to return. It reattaches on the canopy and forms the first vortex-ring. The other passes the margin of bottom parachute and separates to roll in the wind shadow of parachute, which forms the second vortex-ring. The flow field topological structure of this numerical result is consistent with the result in Refs. [15–16].

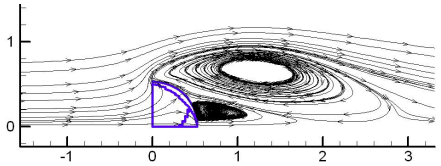

Fig. 7.　Flow lines map on symmetry plane of parachute

The flow lines on symmetry plane of the second example are shown in Fig. 8. As the role of wake flow of projectile, there are not only two vortex-rings at the wind shadow of parachute but also two vortex-rings at the inner of parachute. Due to the existence of these two inner vortex-rings, the pressure of the inner parachute is lower, so that the parachute drag of the second example is less than the first one.

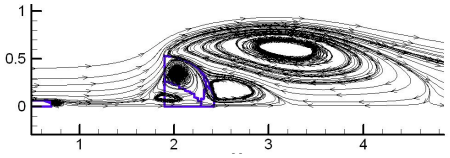

Fig. 8.　Flow lines map on symmetry plane of parachute-projectile

The drag coefficients of parachutes are shown in Table 3.

Table 3. Drag coefficient of CFD (v=15 m/s)

Parachute	Diameter ratio d_{sb}/d_{pb}	Parachute drag coefficient of example (1) C_{d1}	Parachute drag coefficient of example (2) C_{d2}	Coefficient Δ/%	Coefficient k
A	0.122 6	0.642 25	0.516 48	19.58	1.597
B	0.135 4	0.674 52	0.523 81	22.34	1.650
C	0.152 9	0.685 47	0.512 64	25.21	1.649

In Table 3, v is speed. C_{d1} and C_{d2} can be obtained from fluent simulation when the velocity v and parachute area A are set.

$$\Delta = \frac{C_{d2} - C_{d1}}{C_{d1}}, \tag{18}$$

$$k = \frac{\Delta}{d_{sb} / d_{pb}}. \tag{19}$$

The results in Table 3 indicate that the drag of parachutes in the second simulation is smaller compared with the prior one. The influence of projectile wake flow to the parachute flow field cannot be ignored.

The value of k indicates that when the ratio d_{sb}/d_{pb} increases, Δ also increases, and the trend is linear. With the same carrier, the larger of parachute size is, the smaller projectile wake flow influence will cause. For the parachutes with same form and same canopy material in this paper, k is about 1.6.

4 Wind Tunnel Tests Result

For the two examples in section 3, wind tunnel tests are carried out to verify the numerical results. The wind tunnel is vertical and S-type force measure sensor is installed under the parachutes. The installation of the sensors is shown in Fig. 9 and Fig. 10.

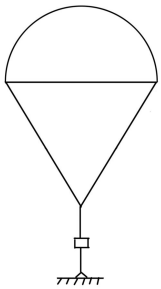

Fig. 9. Sensor installation for parachute

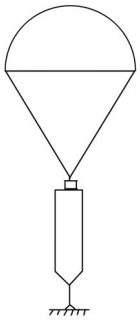

Fig. 10. Sensor installation for parachute-projectile

In the wind tunnel test for parachute alone, the force read from sensor is

$$F_a = D_{pa} - G_p, \tag{20}$$

where D_{pa} is the drag of parachute in the first wind tunnel tests, and G_p is the weight of parachute.

In the wind tunnel test for parachute-projectile, the force read from sensor is

$$F_b = D_{pb} - G_p, \tag{21}$$

where D_{pb} is the drag of parachute in the second wind tunnel tests.

The weight of sensor can be ignored by adjusting the zero point before the tests. Through Eqs. (20) and (21), the drag of parachute in wind tunnel tests can be obtained by subtracted parachute weight from sensors data.

With increasing of flow speed, the parachutes drag under various speeds can be read from the sensor. The parachute opening process and the attitude of parachute and projectile can also be observed. The wind tunnel test of the first example is shown in Fig. 11, and the second example is shown in Fig. 12.

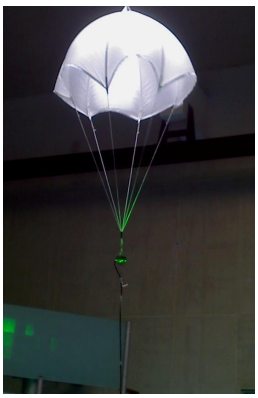

Fig. 11. Wind tunnel tests of parachute

Fig. 12. Wind tunnel test of parachute-projectile

The results from wind tunnel test are shown in Table 4 and Table 5.

Table 4. Wind tunnel results of parachute

Parachute	Speed v/(m • s^{-1})	Drag from sensor D_s/kg			Drag average value D_{a1}/kg	Parachute drag coefficient C_{d1}
		1	2	3		
A	13	8.693	8.584	8.624	8.63	0.613
	14	9.655	9.514	9.593	9.59	0.597
	15	10.937	10.812	10.915	10.88	0.590
B	13	6.745	6.768	6.812	6.78	0.609
	14	7.898	8.087	8.005	8.00	0.619
	15	9.034	9.217	9.125	9.13	0.616
C	13	5.315	5.408	5.451	5.39	0.618
	14	5.986	6.152	6.085	6.07	0.599
	15	6.875	6.957	6.921	6.92	0.596

Table 5. Wind tunnel results of parachute-projectile

Parachute	Speed v/(m • s^{-1})	Drag from sensor D_s/kg			Drag average value D_{a2}/kg	Parachute drag coefficient C_{d2}	Coefficient Δ/%	Coefficient k
		1	2	3				
A	13	7.014	6.942	6.897	6.95	0.501	18.27	1.490
	14	7.702	7.591	7.513	7.60	0.473	20.77	1.694
	15	9.113	8.942	8.914	8.99	0.488	17.29	1.410
B	13	5.512	5.417	5.284	5.40	0.485	20.36	1.504
	14	6.348	6.332	6.012	6.23	0.482	22.13	1.634
	15	7.428	7.395	7.214	7.34	0.495	19.64	1.451
C	13	4.115	3.984	4.012	4.04	0.463	25.08	1.640
	14	4.648	4.513	4.498	4.55	0.450	24.87	1.627
	15	5.705	5.512	5.318	5.51	0.474	20.47	1.339

Through Table 4 and Table 5, the wind tunnel tests results are about 7% less than the CFD numerical results. The reasons for this are given as follows. Firstly, the surface of parachute is set up as wall condition without sliding in CFD simulation, so that the canopy porosity is ignored, additionally, the parachute in real application is not normally hemispherical. Although the CFD numerical result is more than the wind tunnel tests result, both of them have a similar trend. It indicates that using CFD simulation in parachute design is reliable.

The results of wind tunnel tests also prove that the wake flow of projectile affects the parachute flow field obviously. The drag coefficient of parachute-projectile system is about 20% less than the drag coefficient of parachute alone. As the same result with CFD simulation, k value also indicates that as the distance between parachute and projectile is constant and the projectile size is fixed, the larger the parachute becomes the smaller influence by projectile wake flow is. And the k value of these parachutes is 1.339–1.694, also around 1.6, which is the same as CFD simulation results.

5 Conclusions

(1) CFD simulation for parachute flow field is developed in this paper. The wind tunnel tests are carried out to verify the validity of the CFD simulation. The wind tunnel tests results are about 7% less than the CFD numerical results.

(2) Through both the CFD calculation and wind tunnel tests results, since the parachute size is on the same magnitude of projectile, the wake flow of projectile evidently affects the flow field of parachute, which causes the parachute drag decreasing about 20%. In the design of small parachute, the influence of carrier wake flow can not be neglected.

(3) As the distance between parachute and projectile is constant and the projectile size is fixed, the bigger parachute induces smaller influence by projectile wake

flow. When the ratio d_{sb}/d_{pb} increases, the influence also increases, and the trend is linear.

References

[1] YU Li, MING Xiao. Investigation on the characteristics of parachute flow-field[J]. *Acta Aerodynamica Sinica*, 2007, 25(3): 306–310. (in Chinese)

[2] KENNETH J. DESABRAIS. Aerodynamic forces on an airdrop platform[G]. *AIAA Paper*, 2005-1634.

[3] LIU Wei, TANG Qiangang, KOU Baohua. Numerical simulation of velocity and spin speed of parachute-spinning projectile system[J]. *ACTA Armamentarii*, 2007, 28(11): 1 302–1 305. (in Chinese)

[4] DESABRAIS K J, JOHARI H. Unsteady potential flow forces on an inflating parachute canopy[G]. *AIAA Paper*, 2003-2144.

[5] JOHN W WATKINS. A total energy method to predict parachute canopy inflation force[G]. *AIAA Paper*, 2003-2166.

[6] HEIXRICH H G, JAMISON L R. Parachute stress analysis during inflation and at steady state[J]. *Journal of Aircraft*, 1966, 3(1): 52–58.

[7] PENG Yong. *Research and application of some dynamic problem of the recovery system of manned spacecraft*[D]. Changsha: National University of Defense Technology, 2004. (in Chinese)

[8] TANG Qiangang, ZHANG Qingbin, ZHANG Xiaojin. Nine-degree-of-freedom model of bomb-parachute system[J]. *ACTA Armamentarii*, 2007, 28(4): 449–452. (in Chinese)

[9] ZHU Yong, LIU Li. Dynamic model of parachute-projectile systems based on Lagrange mechanics[J]. *ACTA Aeronautica et Astronautica Sinica*, 2009, 30(7): 1 208–1 213. (in Chinese)

[10] KEITH R STEIN, RICHARD J BENNEY, JOHN W LEONARD. Fluid-structure interactions of a round parachute: modeling and simulation techniques[J]. *Journal of Aircraft*, 2001, 38(5): 800–808.

[11] TAYLOR A P. An investigation of the apparent mass of parachutes under post inflation dynamic loading through the use of fluid structure interaction simulation[G]. *AIAA Paper*, 2003-2104.

[12] JOHARI H, DESABRAIS K J. A coupled fluid-structure parachute inflation model[G]. *AIAA Paper*, 2003-2146.

[13] JOHARI H, DESABRAIS K J, LEE C K. Effects of inflation dynamics on the drag of round parachute canopies[G]. *AIAA Paper*, 2007-2562.

[14] CAO Yihua, WANG Kan, YU Ziwen. Numerical simulation of parachute fluid-structure interaction and flow field analysis[G]. *AIAA Paper*, 2007-2573.

[15] JIANG Chongwen, CAO Yihua, SU Wenhan. The flow-field characteristics of an axisymmetric parachute in terminal descent[J]. *Spacecraft Recovery & Remote Sensing*, 2005, 26(3): 10–15. (in Chinese)

[16] JIANG Chongwen, CAO Yihua, SU Wenhan. Influence of circular angle in symmetric plane to the flowfield characteristics of an axisymmetric parachute[J]. *Journal of Beijing University of Aeronautics and Astronautics*, 2006, 32(3): 271–275. (in Chinese)

[17] WANG Kan, CAO Yihua, YU Ziwen. Numerical simulation of parachute fluid-solid coupling problem and flow analysis[J]. *Journal of Beijing University of Aeronautics and Astronautics*, 2007, 33(9): 1 029–1 032. (in Chinese)

[18] SONG Qianfu, CAO Yihua, JIANG Chongwen. Engineering analysis method in fluid-structure interaction problem of hemispherical parachute[J]. *Journal of Beijing University of Aeronautics and Astronautics*, 2009, 35(1): 96–99. (in Chinese)

[19] VLADIMYR GIDZAK, MICHAEL BARNHARDT, TRAVIS DRAYNA. Comparison of fluid-structure interaction simulations of the MSL parachute with wind tunnel tests[G]. *AIAA Paper*, 2009-2971.

Biographical notes

ZHU Yong, born in 1983, is currently a PhD candidate in *School of Aerospace Engineering, Beijing Institute of Technology, China*. He received his bachelor degree from *Beijing Institute of Technology, China*, in 2005. His research interests include flight vehicle design.
Tel: +86-10-68913290; E-mail: zhuyong@bit.edu.cn

LIU Li, born in 1964, is currently a professor in *Beijing Institute of Technology, China*. She received her PhD degree from *Beihang University, China*. Her research interests include flight vehicle design and Structure design.
Tel: +86-10-68911926; E-mail: liuli@bit.edu.cn

WANG Zhengping, born in 1972, is currently a PhD candidate in *School of Aerospace Engineering, Beijing Institute of Technology, China*.
Tel: +86-10-68911926; E-mail: wzp@bit.edu.cn